Model projected changes of extreme wind events in response to global warming

G. Gastineau[1] and B. J. Soden[1]

Received 27 January 2009; revised 20 March 2009; accepted 8 April 2009; published 23 May 2009.

[1] The changes in the frequency of occurrence of extreme wind storm events in response to anthropogenic global warming are explored using a multi-model ensemble of coupled climate model simulations. These changes, diagnosed using several different metrics based on the daily wind fields, indicate that the frequency of the most extreme wind events decreases over the tropics in association with the model-projected weakening of the large-scale atmospheric circulation. At higher latitudes, the strongest near-surface wind events are found to increase in frequency in association with the amplified baroclinicity and poleward shift of the midlatitude storm tracks. The frequency of the heaviest precipitation events increases in all models, despite a systematic reduction of extreme upward vertical velocities, due to the increased moisture content of the lower troposphere. All of these changes are shown to be robust projections of current climate models.
Citation: Gastineau, G., and B. J. Soden (2009), Model projected changes of extreme wind events in response to global warming, *Geophys. Res. Lett.*, *36*, L10810, doi:10.1029/2009GL037500.

1. Introduction

[2] Extreme weather events impact a wide range of social, economic and environmental systems. It is widely believed that certain extreme events, such as heat waves, droughts, and heavy precipitation, have become more common and more severe over the past half-century and are projected to increase further in response to rising concentrations of greenhouse gases [*Climate Change Science Program*, 2008].

[3] Future projections of changes in extreme weather events are based on scenario simulations using state of art coupled models. Certain projections, such as increased frequency of droughts and floods, are directly tied to increase in lower tropospheric moisture, for which our confidence in the model simulations is high [*Held and Soden*, 2006]. The increased moisture leads to a greater transport by the atmosphere from the divergent regions to the convergent regions. The wet regions get wetter, while the dry regions become dryer [*Held and Soden*, 2006; *Chou and Neelin*, 2004]. Extreme rain events are also expected to become more frequent in response to global warming [*Kharin et al.*, 2007; *Lenderink and van Meijgaard*, 2008], although some studies suggest that the model projected changes are weaker than observed [*Allan and Soden*, 2008]. Over subtropical land area, *Tebaldi et al.* [2006] and *Seager et al.* [2008] show that the number of dry days increases, so that the mean precipitation decreases in some regions.

[4] Another consequence of the lower tropospheric moisture increase is a weakening of the large scale tropical circulation, that was diagnosed for the Walker and Hadley circulation [*Zhang and Song*, 2006; *Vecchi and Soden*, 2007; *Held and Soden*, 2006; *Gastineau et al.*, 2008]. However, at high latitudes, coupled model simulations show an increased baroclinicity and a poleward shift of the storm tracks [*Yin*, 2005]. The circulation and precipitation changes modify the character of the precipitation events, and lead, in midlatitudes, to a greater precipitation intensity [*Meehl et al.*, 2005].

[5] After a presentation of the methodology in section 2, the changes in the intensity and frequency of wind storm and precipitation events are first diagnosed globally in section 3, using the multi-model dataset daily outputs. As different large scale circulation changes occur in tropics and high latitudes, the changes are investigated separately for these two regions in section 4. The last section summarizes our findings.

2. Data and Methods

[6] Our analysis is based on daily sea-level pressure, zonal and meridional velocities, temperature and precipitation, retrieved from the multi-model dataset of the World Climate Research Programme's (WCRP) Coupled Model Intercomparison Project Phase 3 (CMIP3). We limit our analysis to the models for which the daily three dimensional zonal and meridional velocities were available: CGCM3.1(T47), CGCM3.1(T63), CSIRO-Mk3.0, CSIRO-Mk3.5, CNRM-CM3, GFDL-CM2.0, GFDL-CM2.1, GISS-AOM, FGOALS-g1.0, INM-CM 3.0, IPSL-CM4, MIROC3.2(hires), MIROC3.2 (medres), MIUB/ECHO-G, ECHAM5/MPI-OM, ECHAM5/INGV and MRI-CGCM2.3.2. Two periods of the IPCC-scenario simulations are studied, (1) the last 5 years of the 20th century simulation, 20C3M, i.e., the period during the years 1995–2000. (2) the last 5 years of the A1B scenario of greenhouse gases emission, i.e., the years 2095–2100.

[7] We use daily precipitation and several different metrics of the daily wind fields to describe changes in storminess in response to increased greenhouse gases. These include the speed and vorticity of the near-surface wind, and the mid-tropospheric vertical velocity. The vorticity is normalized by the sign of the Coriolis parameter $f/|f|$, so that positive (negative) normalized relative vorticity corresponds to cyclonic (anticyclonic) circulation in both hemispheres. Because the models have different vertical

[1]Department of Meteorology and Physical Oceanography, Rosenstiel School for Marine and Atmospheric Science, Miami, Florida, USA.

0094-8276/09/2009GL037500$05.00

resolutions the altitude of the surface wind field can vary among models. We use the near-surface winds at 850-hPa, whose behavior is expected to be closely tied to those at the surface.

[8] The mid-tropospheric vertical pressure velocity is not available in the daily multi-model dataset, and is deduced from the continuity equation:

$$\overline{\omega_{500}} = \frac{dp_s}{dt} + \int_{p_s}^{500} \nabla.\mathbf{V}dp \quad (1)$$

[9] Where, **V** designates the horizontal wind vector. p_s is the surface pressure, p, the pressure and $\overline{\omega_{500}}$, the continuity-derived pressure velocity at 500-hPa. A comparison using those models for which the daily omega field was available confirms that the changes in vertical velocity derived in this way agree well with that computed directly by the models, as illustrated in Figures S1 and S2 of the auxiliary material.[1] Then, the ascending velocity $\overline{\omega_{500}}^+$ is deduced by taking the vertical velocity absolute value and neglecting the subsident values. Lastly, we mask out the regions where the surface pressure is lower than 900-hPa, thus eliminating winds over the main ice sheets and mountain ranges from our analysis.

3. Change in Storminess in Global Warming Conditions

[10] We used the change in frequency of occurrence to diagnose the changes of extreme events. First, the 5^{th}, 10^{th}, ..., 95^{th} and 99^{th} percentiles of precipitation, ascending pressure velocity, surface wind speed and vorticity are calculated, from the last 5 years of the 20C3M simulation. The percentiles bins are computed separately for each grid point, to account for their strong regional dependence. Then, the frequency of occurrence in these percentiles (i.e., defined from the 20C3m simulation) is computed for the last 5 years the A1B scenario for each models (similar to *Vecchi and Soden* [2007] and *Allan and Soden* [2008]). The change in the frequency of occurrence, as a function of the percentile bins, provides a measure of the change in the probability density function for that variable and model Alternatively, one could measure the change in threshold for a specific percentile bin between the 20C3M and A1B simulations. Such an analysis is presented in Figures S3 and S4 of the auxiliary material and yields results consistent with those presented below. The changes in frequency of occurrence for each model are then normalized by corresponding change in global mean surface temperature. Finally, the multi-model mean is calculated using the normalized changes.

[11] Figure 1 (left) gives the global mean changes in frequency of occurrence of the multi-model mean for all four variables: precipitation, 500-hPa ascending velocity, 850-hPa wind speed and 850-hPa vorticity. The coupled models show little change for the lowest precipitation bins (0–50% bins). The moderate precipitation events are less frequent, while the strongest precipitation events are more frequent (>90% bins); for instance the 99–100% bin is found to be 20% more frequent. The decrease in moderate precipitation events is consistent with the upped-ante mechanism [*Chou and Neelin*, 2004]; as the atmosphere is more stable, the precipitation decreases at the edge of the convergent zones. On the other hand, as the atmosphere holds more water vapor, the precipitation intensity increases within the convergent zones, represented by the strongest precipitating bins.

[12] The global changes in frequency of occurrence of the ascending velocity $\overline{\omega_{500}}^+$ show an increase in the weakest updrafts (0–50% bins), while the strongest updrafts become less frequent (60–100% bins). For the wind speed, we also found more weak events (0–45% bins), and less strong events (45–95% bins). However, the most intense wind events (99–100% bin) become more frequent. For reference, the wind percentiles are given in Table S1 of the auxiliary material. The vorticity changes are also associated with an overall weakening, with a global decrease of the rotational component of the wind, as the strong cyclonic and anticyclonic events (80–100% and 0–20% bins respectively) become less frequent while the weak circulation events (20–80% bins) are more frequent.

[13] The robustness of these changes are examined in two different ways. First, the error bars in Figures 1 and 2 indicate the standard deviation among the 17 models used in this study. Second, the upper part of each plot in Figure 1 displays the number of models, out of a total of 17, whose change is of the same sign as the multi-model mean. The changes in the moderate percentile bins are remarkably robust for most models. For the 99–100% bin, the changes are less robust, but they are still represented by at least 12 models out of 17.

[14] In order to study the relationship between heavy the precipitation events and the circulation changes, we bin the wind metrics as a function of the corresponding precipitation intensity. This binning is done using the precipitation percentile thresholds defined from the 20C3M simulation. The ascending velocity, wind speed and cyclonic vorticity for each percentile bin are averaged, for the 20C3M and A1B simulations. For clarity, the anticyclonic vorticities are neglected in the binning of the vorticity. The relative changes between the two simulations are then normalized by the mean surface warming for each models. Figure 2 (left) shows the global relative changes for the multi-model mean. The strongest precipitation bins (>90% bins) are associated with weaker ascending velocity and surface cyclonic vorticity. The wind speed shows only weak changes. This suggests that the increase of the heavy precipitation events in the models results from the increased water vapor and not an increase in the strongest circulation events.

4. Spatial Distribution of Changes in Extreme Wind Events

[15] To examine the regional distribution of the changes in extreme events, Figure 3 shows a map of the relative change in frequency of occurrence for the 95–100% percentile bin for each of the wind metrics and the precipitation. The contours indicate the value of the 95^{th} percentile threshold at each grid point.

[16] The changes in the strong precipitation events are similar to the precipitation change of the models. Within the

[1] Auxiliary materials are available in the HTML. doi:10.1029/2009GL037500.

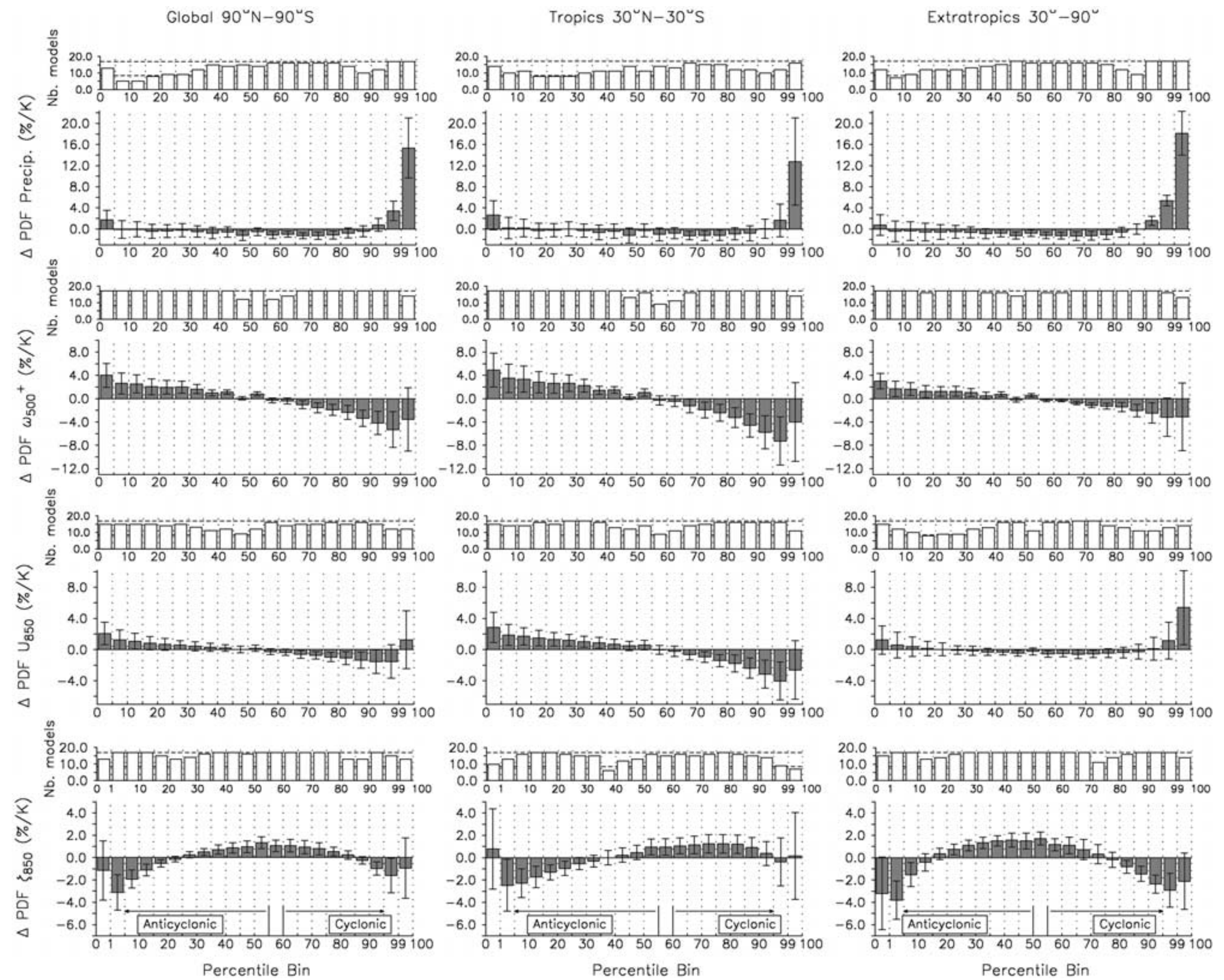

Figure 1. Percentage changes in the frequency of occurrence of precipitation, 500-hPa ascending continuity-derived omega (ω_{500}^{+}), 850-hPa wind speed (U_{850}) and 850-hPa normalized vorticity (ζ_{850}). The results are expressed in % per degree K of surface warming and then averaged across all models to create the multi-model mean. The error bars show the standard deviation among the coupled models. The upper part of each plot gives the number of models with a change of the same sign as the multi-model mean. (left) Global changes, (middle) tropical (30°N–30°S) and (right) extratropical (30°–90°) changes.

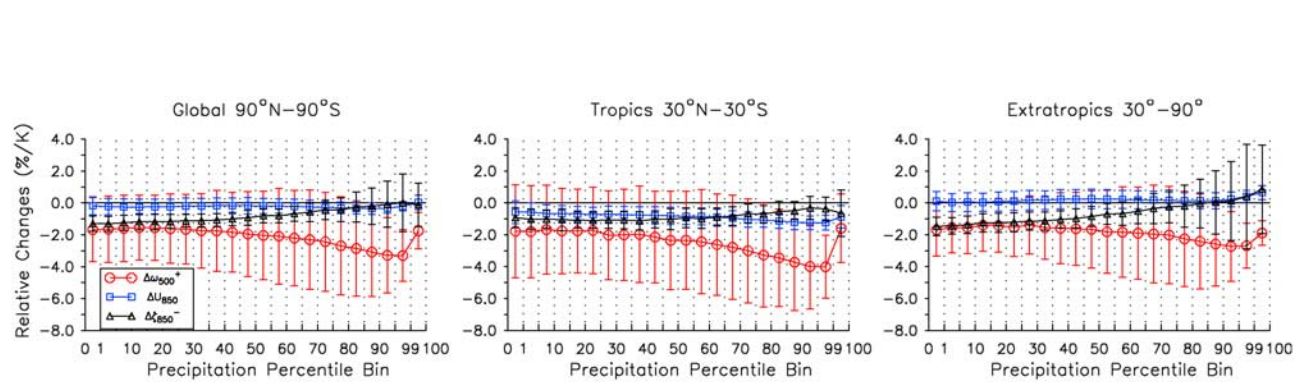

Figure 2. Relative changes of the 500-hPa ascending velocity, 850-hPa wind speed and normalized cyclonic vorticity (ζ_{850}^{-}), averaged as a function of the corresponding precipitation percentile bins. The changes are calculated using the last 5 years of the A1B and the 20C3M scenarios. The results are expressed in % per degree K of surface warming and then averaged across all models to create the multi-model mean. The errors bars indicate the inter-model standard deviations. A threshold of 0.05 mm/d was used to derive the precipitation changes. (left) Global, (middle) tropical, and (right) extratropical changes.

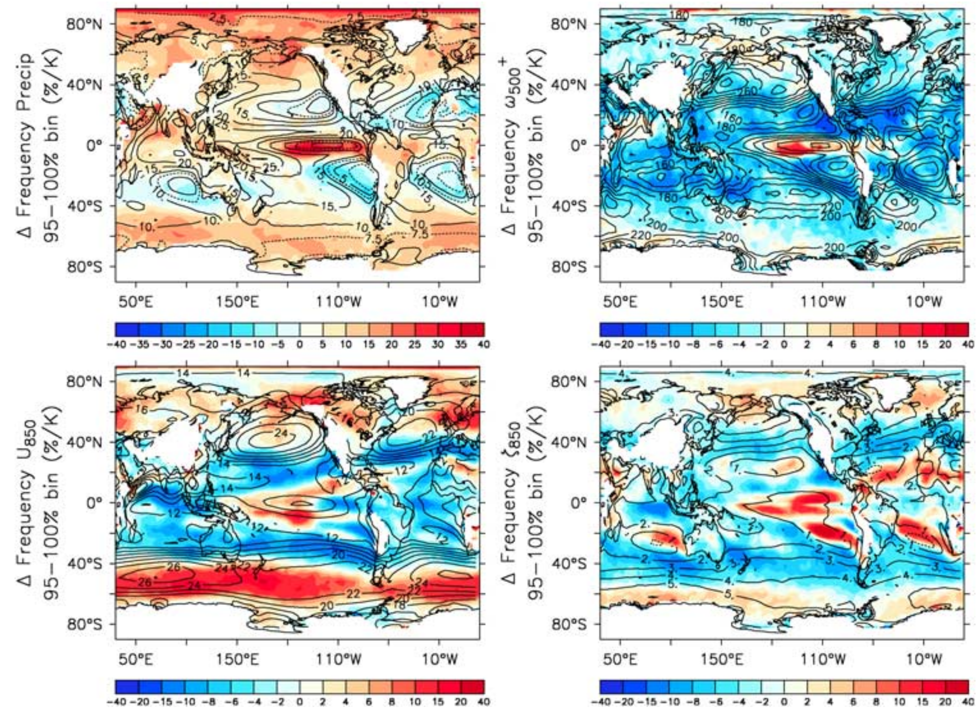

Figure 3. Relative changes in frequency of occurrence for the 95–100% percentile bin (color), in % per degree K of surface warming, from the multi-model mean, for precipitation, 500-hPa ascending velocity, 850-hPa wind speed and 850-hPa normalized vorticity. The contours depict the value of the 95^{th} percentile bin, the corresponding units are respectively mm d^{-1}, hPa d^{-1}, m s^{-1} and s^{-1}. Dash lines show the half intervals of the contours.

ITCZ and in midlatitudes, strong precipitations events are more frequent. In the subtropical regions where the 95^{th} percentile is the smallest, the most intense precipitation events decrease in frequency.

[17] The frequency of the strongest ascending velocity decreases globally. One exception is found in the central and eastern Pacific Ocean, which corresponds to an area of increased convection associated with an El-Niño like pattern of warming [*Vecchi and Soden*, 2007]. The frequency of the strongest wind events decreases between 40°N and 40°S, again with the exception of the central Pacific Ocean. In the tropics and subtropics, the decrease in the extreme surface wind events agrees with the decrease in the mean wind. The trade winds are weaker and shifted polewards in most regions, as illustrated in Figure S5 of the auxiliary material. However, the strongest wind events are more frequent in the storm-track regions, around the 60° latitudes in both hemispheres, and they shift polewards with the poleward movement of the storm tracks. We note that high and low-pass filtered wind speed shows similar changes, and the wind changes are due to both the mean and the eddy components in similar proportions.

[18] The strongest cyclonic vorticities also become less frequent between 50°N and 50°S. In some tropical regions, where the 95^{th} normalized-vorticity percentile is a minimum, the occurrence frequency of the strongest cyclonic events increases. The increased frequency is mainly associated with a poleward shift of the subtropical oceanic sea-level pressure anticyclones, while in the Central Pacific, it is associated with the increased convection. The strongest cyclonic events are also more frequent in polar latitudes, where the 95^{th} percentile is the strongest, which is again consistent with a poleward shift and an intensification in the high latitudes circulation structures.

[19] The changes in position and intensity of the storm tracks have been previously attributed to the enhanced baroclinicity in this region, induced by the meridional SST changes [*Yin*, 2005]. The reason of these changes is still unclear, *Von Storch* [2008] further noted that a positive feedback enhances the atmospheric circulation over the Southern Ocean. The increase in surface wind stress strengthens the Ekman transport which in turn maintains a strong SST meridional gradient.

[20] Based on the spatial patterns noted above, the global mean changes in frequency occurrence shown in Figure 1 (left) are re-computed separately for the tropics (30°N–30°S) and the extratropics (30°–90° in both hemispheres). The results are illustrated in Figures 1 (middle), 1 (right). The precipitation changes are fairly similar for tropics and extratropics, but the circulation changes are different. In the tropics, both the upward vertical velocity and surface wind speed show a decrease in the most extreme events, consistent with the model-projected weakening of the time-mean large scale tropical circulation. On the other hand, the strongest wind events (>95% bins) become more frequent in the extratropics, consistent with the increased baroclinicity in these regions. Similarly, Figure 2 (middle) and 2 (right) shows that the most intense precipitation events are associated with a decrease in near-surface wind and cyclonic vorticity in the tropics, while a small increase is shown for both quantities in the extratropics. In both the tropics and extratropics, the heaviest precipitation events are associated with a reduction in the mid-tropospheric upward vertical velocity, indicating that the model-projected

increase in heavy precipitation is not directly linked to an increase in updraft strength.

5. Summary

[21] This study examines the changes in the frequency of extreme wind storm events in response to anthropogenic global warming, with a multi-model data set of coupled climate model simulations. Using several different metrics based on the daily wind fields, we find that the frequency of the most extreme wind events decreases over the tropics consistent with a reduction in the time mean Walker and Hadley circulations noted in previous modeling studies [*Zhang and Song*, 2006; *Vecchi and Soden*, 2007; *Held and Soden*, 2006; *Gastineau et al.*, 2008]. The heaviest precipitation events are found to become more frequent globally, but are associated with a reduction in upward vertical velocity. The frequency of extreme near-surface wind speed decreases in the tropics but increases in the extratropics in response to global warming. This extratropical increase appears to be associated with the intensification and poleward shift of the midlatitude storm tracks. All of these changes are found to be common projections in current models.

[22] While this study has demonstrated the robustness of changes in extreme wind events in model projections, the veracity of these projections remains an important area for further research. For instance, ocean wind wave data show trends that have similarities with the surface wind change of the models [*Gulev and Grigorieva*, 2004]. There is relatively little long-term observational data that can provide objective direct measures of wind storm intensity. The growing archive of surface wind observations from satellite may offer a useful source of internal or externally-forced variability that can be used to test model projections.

[23] **Acknowledgments.** We thank three anonymous reviewers for helping to improve the manuscript. We acknowledge the modeling groups, the Program for Climate Model Diagnosis and Intercomparison (PCMDI) and the WCRP's Working Group on Coupled Modeling (WGCM) for their roles in making available the WCRP CMIP3 multi-model dataset. Support of this dataset is provided by the Office of Science, U.S. Department of Energy. This research was supported by the NOAA Climate Program Office.

References

Allan, R. P., and B. J. Soden (2008), Atmospheric warming and the amplification of precipitation extremes, *Science*, *321*, 1481–1484, doi:10.1126/science.1160787.

Chou, C., and J. D. Neelin (2004), Mechanisms of global warming impacts on regional tropical precipitation, *J. Clim.*, *17*, 2688–2701.

Climate Change Science Program (2008), Climate models: An assessment of strengths and limitations: A report by the U.S. Climate Change Science Program and the Subcommittee on Global Change Research, Off. of Biol. and Environ. Res., Dep. of Energy, Washington, D. C.

Gastineau, G., H. L. Treut, and L. Li (2008), Hadley circulation changes under global warming conditions indicated by coupled climate models, *Tellus, Ser. A*, *60*, 863–884.

Gulev, S. K., and V. Grigorieva (2004), Last century changes in ocean wind wave height from global visual wave data, *Geophys. Res. Lett.*, *31*, L24302, doi:10.1029/2004GL021040.

Held, I. M., and B. J. Soden (2006), Robust responses of the hydrological cycle to global warming, *J. Clim.*, *19*, 5686–5699.

Kharin, V., F. Zwiers, X. Zhang, and G. Hegerl (2007), Changes in temperature and precipitation extremes in the IPCC ensemble of global coupled model simulations, *J. Clim.*, *20*, 1419–1444.

Lenderink, G., and E. van Meijgaard (2008), Increase in hourly precipitation extremes beyond expectations from temperature changes, *Nat. Geosci.*, *1*, 511–514.

Meehl, G. A., J. M. Arblaster, and C. Tebaldi (2005), Understanding future patterns of increased precipitation intensity in climate model simulations, *Geophys. Res. Lett.*, *32*, L18719, doi:10.1029/2005GL023680.

Seager, R., et al. (2008), Model projections of an imminent transition to a more arid climate in southwestern North America, *Science*, *316*, 1181–1184.

Tebaldi, C., J. M. Arblaster, K. Hayhoe, and G. A. Meehl (2006), Going to the extremes: An intercomparison of model-simulated historical and future changes in extreme events, *Clim. Change*, *79*, 185–211.

Vecchi, G., and B. Soden (2007), Global warming and the weakening of the tropical circulation, *J. Clim.*, *20*, 4316–4340.

Von Storch, J.-S. (2008), Toward climate prediction: Interannual potential predictability due to an increase in CO_2 concentration as diagnosed from an ensemble of AO GCM integration, *J. Clim.*, *21*, 4607–4628.

Yin, J. H. (2005), A consistent poleward shift of the storm tracks in simulations of 21st century climate, *Geophys. Res. Lett.*, *32*, L18701, doi:10.1029/2005GL023684.

Zhang, M., and H. Song (2006), Evidence of deceleration of atmospheric vertical overturning circulation over the tropical Pacific, *Geophys. Res. Lett.*, *33*, L12701, doi:10.1029/2006GL025942.

G. Gastineau and B. J. Soden, Department of Meteorology and Physical Oceanography, Rosenstiel School for Marine and Atmospheric Science, 4600 Rickenbacker Causeway, Miami, FL 33149, USA. (ggastineau@rsmas.miami.edu)